Biomedicine & Pharmacotherapy 121 (2020) 109601

Contents lists available at ScienceDirect

Biomedicine & Pharmacotherapy

journal homepage: www.elsevier.com/locate/biopha

Pharmacology and preclinical validation of a novel anticancer compound targeting PEPCK-M

Marc Aragó[a], Juan Moreno-Felici[a], Sonia Abás[b], Sergio Rodríguez-Arévalo[b], Petra Hyroššová[a], Agnes Figueras[c], Francesc Viñals[a,c], Belén Pérez[d], Maria I. Loza[e], Jose Brea[e], Pedro Latorre[f], Jose A. Carrodeguas[f], Pablo M. García-Rovés[a], Carlos Galdeano[g], Tiziana Ginex[h], Francisco J. Luque[h], Carmen Escolano[b], Jose C. Perales[a,*]

[a] Department of Physiological Sciences, School of Medicine, University of Barcelona, L'Hospitalet del Llobregat, Spain
[b] Laboratory of Medicinal Chemistry (Associated Unit to CSIC), Faculty of Pharmacy and Food Sciences, and Institute of Biomedicine (IBUB), University of Barcelona, Barcelona, Spain
[c] Programs of Molecular Mechanisms and Experimental Therapeutics in Oncology (ONCOBell), and Cancer Therapeutics Resistance (ProCURE), Catalan Institute of Oncology, Bellvitge Institute for Biomedical Research (IDIBELL), L'Hospitalet del Llobregat, Spain
[d] Department of Pharmacology, Therapeutic and Toxicology, Autonomous University of Barcelona, Bellaterra, Spain
[e] Innopharma Screening Platform, BioFarma Research Group, Centro de Investigación en Medicina Molecular y Enfermedades Crónicas (CIMUS), Universidad de Santiago de Compostela, Santiago de Compostela, Spain
[f] Instituto de Biocomputación y Física de Sistemas Complejos (BIFI), BIFI-IQFR (CSIC), Departamento de Bioquímica y Biología Molecular y Celular, Facultad de Ciencias, Universidad de Zaragoza, Zaragoza, Spain
[g] Department of Pharmacy, Pharmaceutical Technology and Physical Chemistry, School of Pharmacy, and Institute of Biomedicine (IBUB), University of Barcelona, Barcelona, Spain
[h] Department of Nutrition, Food Sciences and Gastronomy, School of Pharmacy and Food Sciences, Institute of Biomedicine (IBUB), and Institute of Theoretical and Computational Chemistry (IQTCUB), University of Barcelona, Santa Coloma de Gramanet, Spain

ARTICLE INFO

Keywords:
PEPCK-M
Xanthine derivatives
PEPCK inhibitors
Cancer metabolism
Xenograft
Gluconeogenesis
Breast carcinoma
Colon carcinoma
Preclinical
Mitochondrial physiology
CETSA
Insulin secretion

ABSTRACT

Background: Phosphoenolpyruvate carboxykinase (PEPCK) catalyzes the decarboxylation of oxaloacetate to phosphoenolpyruvate. The mitochondrial isozyme, PEPCK-M is highly expressed in cancer cells, where it plays a role in nutrient stress response. To date, pharmacological strategies to target this pathway have not been pursued.

Methods: A compound embodying a 3-alkyl-1,8-dibenzylxanthine nucleus (iPEPCK-2), was synthesized and successfully probed *in silico* on a PEPCK-M structural model. Potency and target engagement *in vitro* and *in vivo* were evaluated by kinetic and cellular thermal shift assays (CETSA). The compound and its target were validated in tumor growth models *in vitro* and in murine xenografts.

Results: Cross-inhibitory capacity and increased potency as compared to 3-MPA were confirmed *in vitro* and *in vivo*. Treatment with iPEPCK-2 inhibited cell growth and survival, especially in poor-nutrient environment, consistent with an impact on colony formation in soft agar. Finally, daily administration of the PEPCK-M inhibitor successfully inhibited tumor growth in two murine xenograft models as compared to vehicle, without weight loss, or any sign of apparent toxicity.

Conclusion: We conclude that iPEPCK-2 is a compelling anticancer drug targeting PEPCK-M, a hallmark gene product involved in metabolic adaptations of the tumor.

1. Background

Phosphoenolpyruvate carboxykinase (PEPCK) (GTP; EC 4.1.1.32) catalyzes the GTP-dependent conversion of oxaloacetate (OAA) to phosphoenolpyruvate (PEP) from two very similar isozymes localized to the cytosol (PEPCK-C) or the mitochondria (PEPCK-M) [1,2], and

Abbreviations: PEPCK, phosphoenolpyruvate carboxykinase; 3-MPA, 3-mercaptopicolinic acid; PEP, phosphoenolpyruvate; OAA, oxaloacetate; MA, malic acid; GSIS, glucose stimulated insulin secretion; AARE, amino acid response element; ER, endoplasmic reticulum; CETSA, cellular thermal shift assay; ITDRF, isothermal dose-response fingerprint; ADMET, absorption, distribution, metabolism, excretion, and toxicity; BBB, blood brain barrier

* Corresponding author at: Professor "Serra Hunter", School of Medicine, University of Barcelona, 08907, Barcelona, Spain.
E-mail address: jperales@ub.edu (J.C. Perales).

https://doi.org/10.1016/j.biopha.2019.109601
Received 22 July 2019; Received in revised form 24 October 2019; Accepted 25 October 2019

encoded by different nuclear genes (PCK1 and PCK2, respectively). Interestingly, both isozymes are differentially expressed and regulated. Whereas PEPCK-C is restricted to gluconeogenic and glyceroneogenic tissues (liver, small intestine, kidney cortex, and adipose tissue), and responds to insulin, glucagon and dexamethasone, PEPCK-M mRNA content is not regulated by hormonal cues, but it is more widely expressed (*i.e.*, T- and B-cells, pancreatic β-cells, liver, neurons, and undifferentiated tissues such as embryonal stem cells and tumors) [3–8]. In differentiated tissues PEPCK-M role is not completely understood, although it clearly impinges on cataplerosis and TCA cycle flux in the liver [6], and pancreatic β-cells [5].

In tumor cells, on the other hand, this enzyme promotes amino-acid homeostasis, 1-carbon metabolism and several biosynthetic processes crucial to sustain cancer cell and neuroprogenitor metabolism [8–10]. Indeed, the gene encoding for PEPCK-M, PCK2, is a target for ATF4, the master regulator of ER- and amino-acid stress responses [7]. PEPCK-M protein and mRNA was upregulated by effectors of this pathway by recruiting ATF4 to a consensus AARE site located at the PCK2 proximal promoter. Consistently, knocking-down PEPCK-M under stress tipped the balance of the cell towards apoptosis, whereas overexpressing PEPCK-M enhanced cell survival [7]. The importance of chronic ER-stress to induce adaptive responses in cancer cells *in vivo* suggested that the pathway is crucial to cancer cell metabolism and progression. In agreement with this view, loss-of-function genetic models have shown the relevance of PEPCK-M in cell growth and chemoresistance in lung and colon cancer, respectively [10–12].

Thus, we have aimed to identify the potential for this pathway in cancer therapeutic intervention by evaluating a small molecule targeting this enzyme, and its pharmacological validation in a murine preclinical cancer indication. A compound embodying a 3-alkyl-1,8-dibenzylxanthine skeleton previously described as GTP competitive inhibitor for PEPCK-C [13] in an *in vitro* assay, was retargeted against PEPCK-M and systematically assessed for target engagement, efficacy *in vitro*, and pharmacokinetics and activity *in vivo*. PEPCK-M inhibition leads to metabolic imbalances comparable to down-regulation of the enzyme using genetic models (*i.e.*, CRISPR/*cas*9), hindering cell viability *in vitro* and in xenograft models of transformed embryonal kidney (HEK-293) and colon carcinoma (SW-480) tumor growth. Therefore, we conclude that the PEPCK-M inhibitor described here have potent anticancer activities, underscoring the potential of this pathway as a novel therapeutic target.

2. Methods

2.1. Synthesis

The details of the synthesis and characterization of iPEPCK-2 are given in Methods S1 in Supporting Information.

2.2. Computational protocol

Pairwise sequence alignment for PEPCK-C and PEPCK-M isoforms was performed using stretcher (https://www.ebi.ac.uk/Tools/psa/; see Fig. S2 in Supporting Information). The PDB structure of human PEPCK-C co-crystallized with the GDP-competitive inhibitor, *N*-(4-{[3-butyl-1-(2-fluorobenzyl)-2,6-dioxo-2,3,6,7-tetrahydro-1*H*-purin-8-yl] methyl}phenyl)-1-methyl-1*H*-imidazole-4-sulfonamide (PDB ID: 2GMV) [13] was used as a template to generate the protein model for PEPCK-M with Swissmodel [14]. Choice of this X-ray structure was motivated by the high resemblance between the crystallographic ligand and iPEPCK-2.

AutoDock4 [15] was used to dock iPEPCK-2 in PEPCK-M generated by homology modeling from the cytosolic isoform. A structural water molecule (wat740 in 2GMV), mediating ligand interactions with protein residues W527 and W516, was included in the PEPCK-M structure, and its position was determined upon alignment of the 3D structures of the homology model built for PEPCK-M and the reference PDB (2GMV) structure. A grid spacing of 0.375 Å was used in conjunction with 62 × 62 × 62 grid points to define the box considered to explore the arrangement of the ligand in the binding pocket. A genetic algorithm was used to guide the docking search during pose generation. A total of 30 docking conformations were finally generated and analyzed.

2.3. Recombinant human PEPCK-C and PEPCK-M

Open reading frames from human PCK1 coding for PEPCK-C and PCK2 coding for PEPCK-M were cloned and transferred to the pET15b vector, and competent BL21 *E. coli* cells were transformed with the expression construct. Cells were precultured in 10 mL of 2xYT overnight, and the next day were grown at 37 °C in 200 mL of 2xYT medium until they grew to an optical density of 0.5-0.6 at λ_{600}. Then, IPTG was added to a final concentration of 1 mM to induce protein expression. The cells were incubated at room temperature for 5 h under moderate shaking (110 rpm). PEPCK-M was produced and isolated from Arctic express *E. coli* cells as described [16].

Cells were harvested by centrifugation and resuspended in lysis buffer, then lysozyme was added, and the mix was incubated 30 min in ice. The suspension was sonicated on ice for six cycles of 10 s ON and 30 s OFF. Then, DNAse was added, and after 15 min incubation, the cell debris was removed by centrifugation and the supernatants were purified using Qiagen Ni-NTA Agarose following the manufacturer protocol. The purified enzymes were used immediately or stored at −80 °C until needed.

2.4. PEPCK activity assays

Kinetic assays were performed analyzing NADH consumption by spectrophotometry. Absorbance was measured at 340 nm during 6 min at 37 °C in a total volume of 1 mL. The following reaction was studied in the presence of different concentrations of PEPCK inhibitors:

$$PEP + CO_2 + GTP \ (PEPCK) \rightarrow GDP + OAA + NADH \ (MDH) \rightarrow MA + NAD^+$$

The reaction was performed in 50 mM Tris-HCl (pH 7.4), 20 mM $NaHCO_3$, 1 mM $MnCl_2$, in the presence of CO_2 (carbogen infusion for 10 min). Then the following components were added: 0.5 mM PEP, 0.1 mM NADH, 2 UI/mL Malate dehydrogenase (MDH), 5 μM rotenone, 25 mM DTT. Recombinant PEPCK-C or PEPCK-M and the inhibitors were then added, and the reaction started by the addition of 0.2 mM of GDP.

2.5. Cell culture

All cell lines, except otherwise indicated, were grown in DMEM medium supplemented with 10% of fetal bovine/calf serum, 100 IU/mL penicillin + 100 μg/mL streptomycin, and 2 mM glutamine. INS-1 rat insulinoma cells were grown in complete RPMI-1640 supplemented with 71 μM of β-mercaptoethanol. For glucose deprivation experiments cells were seeded with glucose-free DMEM, and it was supplemented with 10% of dialyzed FBS, 100 IU/mL penicillin + 100 μg/mL streptomycin, and 2 mM glutamine.

2.6. Cellular thermal shift assay (CETSA)

Intact and viable mouse embryonal fibroblast (MEF) cells were harvested and resuspended to a final concentration of 2×10^6 cells/mL. Different PEPCK-M inhibitors were added to this suspension, to a final concentration of 5 μM, and incubated for 30 min at 37 °C. Cells were washed and resuspended with PBS to a final concentration of 3×10^7 cells/mL. They were split in different tubes and treated with a gradient of temperatures between 40 and 60 °C for 3 min, cells were incubated

3 min at room temperature and snap frozen with liquid nitrogen. Cells were lysed using a freeze/thaw cycle with liquid nitrogen and centrifuged at 20000 *g* 20 min at 4 °C. Finally, stable PEPCK-M present in the supernatant was quantified by western blot.

The analysis was also performed treating the cells with a gradient of PEPCK-M inhibitor concentrations and a thermal treatment at a single temperature (60 °C). IsoThermal Dose-Response Fingerprint ($ITDRF_{CE\text{-}TSA}$) concentrations were calculated as described [17].

2.7. Cell viability and anchorage-independent growth

Proliferation assays were performed on MCF7, HEK-293, HCT-116 and SW-480 cells seeded at 5×10^3 cells/well in 96-well plates. After overnight incubation cells were treated with the different PEPCK inhibitors between 24 and 72 h. Then viability was measured by MTT.

Anchorage-independent growth capacity was tested counting the colonies formed when cells have been seeded in soft agar. Firstly, the wells of 6-well plates were filled with 2 mL of complete medium with 0.6% melted agar. When agar solidified, 10^5 cells were seeded in 1 mL of complete medium (DMEM) with 0.3% agar with or without PEPCK-M inhibitors. Once the superior layer solidified, 500 μL of treatment medium was renewed, and changed twice a week. The plate was incubated for two weeks, and the colonies were stained with MTT and counted.

2.8. Glucose-stimulated insulin secretion (GSIS)

Insulin secretion experiments were performed in INS-1 rat insulinoma cells and fasted ICR mice. GSIS in INS1 cells; four hundred thousand cells/well were seeded in a 24 well and incubated with 2.8 mM of glucose KRBH medium in the presence or absence of iPEPCK-2 for 2 h. Then, the medium was discarded and 500 μL of KRBH medium with 2.8 mM of glucose were added for 1 h. Next, supernatants were collected and incubated in 500 μL of KRBH medium with 16.7 mM of glucose for 1 h. Finally, cells were lysed with RIPA and total protein was quantified for normalization. GSIS in fasted ICR mice; a GSIS assay was performed in male ICR white mice between 30 and 40 g (at least n = 4 per group given that insulin concentrations are quite dispersed in the population at baseline) and all animals were randomized to either the experimental and control groups. A single intraperitoneal dose of iPEPCK-2 (dissolved in 40 % PEG 400 in physiological saline), was administered at the described doses in the morning (between 8 and 10 a.m.) without anesthesia. Later (2 h or 5 h), a bolus of glucose (2 g/kg) was administered *via* IP to induce insulin secretion. Mice were monitored for signs of pain or distress during the time between either injection and euthanasia (at the earliest time of 15 min and the latest at 1 h after glucose bolus injection). Blood (50 μL) was collected from the tail vein after incision at the stated time points, and animals were subsequently sacrificed by cervical dislocation. The content of insulin of the different supernatants (*basal* in 2.8 mM glucose, or *GSIS* in 16.7 mM glucose) was measured by ELISA using the *Mercodia Mouse Insulin ELISA* kit.

2.9. Pharmacokinetics

The pharmacokinetic study was carried on in male ICR white mice between 30 and 40 g (n = 4 per group, which is a small cohort based on the potency of the analytical and quantification techniques utilized) and all animals were randomized to either the experimental and control groups. A single intraperitoneal dose of iPEPCK-2 (dissolved in 40 % PEG 400 in physiological saline), was administered at 8 mg/kg early in the morning (between 8 and 10 a.m.) without anesthesia. Mice were monitored for signs of pain or distress during the time between injection and euthanasia (at the earliest time of 15 min and the latest at 8 h after injection) and sacrificed by cervical dislocation for blood and brain collection. Brain and plasma were immediately frozen at -80 °C for pK analysis. iPEPCK-2 was extracted from plasma and homogenate brain in PBS with acetonitrile, in the presence of 1 M DTT and quantified by HPLC/UV. The solid phase was C18 RP column (5 m, 20 × 0.4 cm; Kromasil 100; Teknokroma) and the mobile phase consisting in a 0.05 M KH_2PO_4 (45%): acetonitrile (55%). The elution time of iPEPCK-2 was 3.7 min, and it was detected at 290 nm. The assay had a range of 0.125–5 μg/mL. Calibration curves were constructed by plotting the peak area ratio of analyzed peak against known concentrations.

iPEPCK-2 plasma concentrations *versus* time curves for the mean of animals were analyzed by a non-compartmental model based on statistical moment theory using the "PK Solutions" computer program. The pharmacokinetic parameters calculated were the area under the concentration *vs* time curve (AUC), which was calculated using the trapezoidal rule in the interval 0–8 h, and the half-life ($t_{1/2\beta}$), which was determined as ln2/β (β was calculated from the slope of the linear, least-squares regression line). The C_{max} and T_{max} were read directly from the mean concentration curves.

2.10. Xenograft subcutaneous models

Two subcutaneous tumor xenograft models were generated by injecting transformed cells in both flanks of female 5–6-week-old BALB/c nude mice (at least n = 5 per group, given the large dispersion on the size of the tumors grown in flanks of immunocompromised mice). In the first model, 1×10^6 HEK-293 cells were injected per flank; whereas on the colon carcinoma model, 5×10^6 SW-480 cells were utilized. Handling for the injections was in the absence of anesthesia or analgesia, and no signs of distress or pain were evident afterwards. Mice were monitored for signs of cancer disease, pain or distress during the time of the experiment and sacrificed by cervical dislocation and removed from the experiment if so advised by the Veterinarian in charge of the animal facility. When the tumors grew enough to be measured, mice were randomly split in two groups, and kept in grouped cages of at least 4 animals per cage. One group received a daily (between 8 and 10 a.m.) IP injection with 8 mg/kg of iPEPCK-2 without analgesia. No signs of distress or pain resulted from the injection. The other group was treated with vehicle (20% PEG400. 5% DMSO, H_2O) instead, following the same therapeutic regimen. The tumors were measured, and mice weighted twice a week. After 15 days (SW-480) or 24 days (HEK-293), mice were euthanized by cervical dislocation, and the tumors and organs processed for further analysis.

2.11. Histopathology

Tissues were fixed twelve hours in 4% Paraformaldehyde Buffer after trimming them into appropriate size and shape and placing them in histology cassettes. They were then dehydrated following an ethanol gradient process and embedded in paraffin. Tissue sections (3–4 μM) were stained with Harris hematoxylin & eosin stain for morphological analysis.

2.12. Statistics and data analysis

Cohort size (greater than 5 per group) for all experiments were based on statistical power calculations using GraphPad Prizm. Animals studies were not replicated to avoid utilization of additional animals and given that a sufficient number of animals in each group was utilized to provide good statistical power. All data was analyzed for variance and represented as means ± standard error of the mean (SEM) for at least 3 independent experiments with 3–8 replicates per group. One-way analysis of the variance (ANOVA) was utilized to unmask significant differences, and a Sidak multiple comparison test was used when indicated in assays containing more than two group comparisons. Minimum statistical significance was set at $*p < 0.05$.

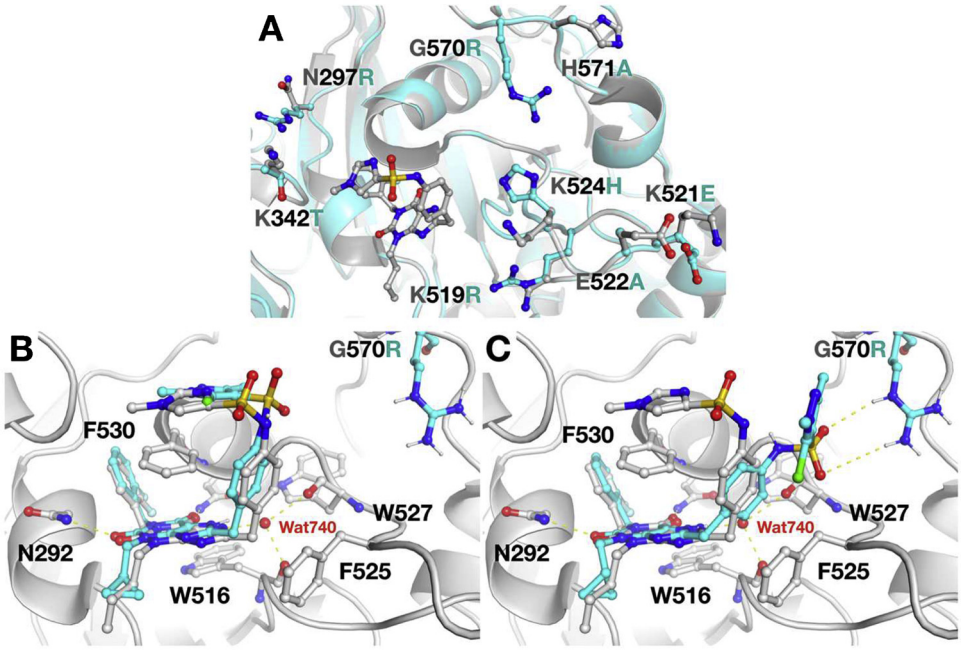

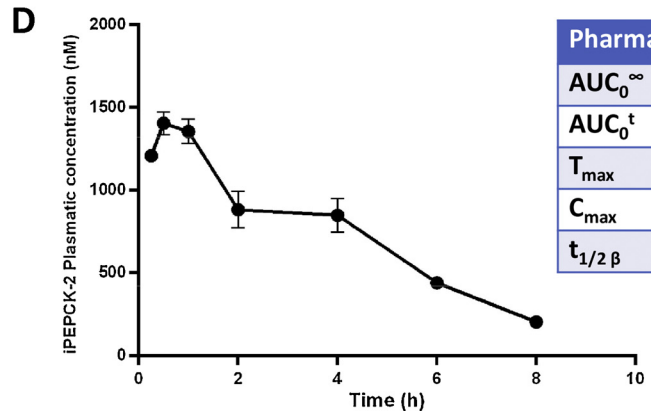

Pharmacokinetic parameters	
AUC_0^{∞}	238.2 μg*min/ml
AUC_0^{t}	218.7 μg*min/ml
T_{max}	0.5 h
C_{max}	0.86 μg/ml
$t_{1/2\,\beta}$	1.8 h

Fig. 1. Docking and pharmacokinetics (A) Superposition of human PEPCK-C (PDB ID: 2GMV; grey) and human PEPCK-M (in cyan). Changes in residue content at/around the binding pocket are highlighted, and the crystallographic pose of the inhibitor (N-(4-{[3-butyl-1-(2-fluorobenzyl)-2,6-dioxo-2,3,6,7-tetrahydro-1H-purin-8-yl]methyl}phenyl)-1-methyl-1H-imidazole-4-sulfonamide) is shown as sticks. (B, C) Representative docking poses for iPEPCK-2 (in cyan) in the GDP-binding site. The reference crystallographic protein-ligand complex (PDB ID: 2GMV) is shown in grey. The G570R mutation is highlighted in cyan/blue. Numbering of residues based on the sequence of PEPCK-C. (D) Plasma concentration of iPEPCK-2 at various times (15 min to 8 h) after an intraperitoneal administration of 8 mg/kg, as determined by HPLC/UV-VIS at 290 nm. Basic pharmacokinetic parameters are shown (in-chart panel). Data are means ± SEM (n = 4 in each time point for panel D).

3. Results

3.1. iPECK-2 is a potent on-target inhibitor of PEPCK-M with drug-like characteristics

We prepared and fully characterized (see Methods S1) 5-chloro-*N*-{4-[(3-(cyclopropylmethyl)-1-(2-fluorobenzyl)-2,6-dioxo-2,3,6,9-tetrahydro-1*H*-purin-8-yl)methyl]phenyl}-1,3-dimethyl-1*H*-pyrazole-4-sulfonamide (iPEPCK-2; chemical structure in Fig. S1 in Supporting Information) previously described by Pietranico et al. as a potent inhibitor of PEPCK-C [13].

The PDB structure of human PEPCK-C co-crystallized with a GTP-competitive inhibitor (PDB ID: 2GMV), was used as template to generate the structural model of PEPCK-M, taking advantage of the high sequence identity (69 %) and similarity (82 %) between the two isoforms (see Fig. S2 in Supporting Information). Superposition of the reference PDB structure for PEPCK-C, and the homology model built for PEPCK-M is shown in Fig. 1A. This comparison highlighted the preservation of residues in the binding pocket, and a few differences in residues around the edges of the pocket filled by the crystallographic ligand. Among them, K342T, K524H, K529R, and G570R are located at less than 8 Å from the ligand in the GDP-binding site. Autodock4 was used to dock iPEPCK-2 in the GDP-binding site of PEPCK-M. The two most interesting docking poses found for iPEPCK-2 are reported in Fig. 1B and C. The xanthine moiety is stably placed in a sub-cavity surrounded by N292, W516, F525, W527, and F530. The two oxygen atoms participate in hydrogen-bonding interactions with N292 and N533. Water-mediated polar interactions are also observed between the protonated nitrogen of the xanthine scaffold and the backbone oxygens of W527 and W516. The 2 F-benzene is inserted in a subpocket and stabilized by hydrophobic interactions with L293 and M296 (not shown). Two different orientations were, however, found for the pyrazole-4-sulfonamide moiety. In one case (Fig. 1B), this fragment matches the arrangement found in the crystallographic ligand in 2GMV, which involves the stacking of the pyrazole ring with F530. In the second case (Fig. 1C), a key difference in the vicinity of the binding pocket is the sulfonamide group interaction exclusive for the guanidine moiety of R570 in PEPCK-M (G570 in PEPCK-C).

Before evaluating iPEPCK-2 as an on-target inhibitor of PEPCK-M *in vitro* and *in vivo*, we performed basic ADMET and pharmacokinetic studies. *In vitro* ADMET assays showed good human and murine microsomal stability with a half-life of 119 min and a 75% of compound

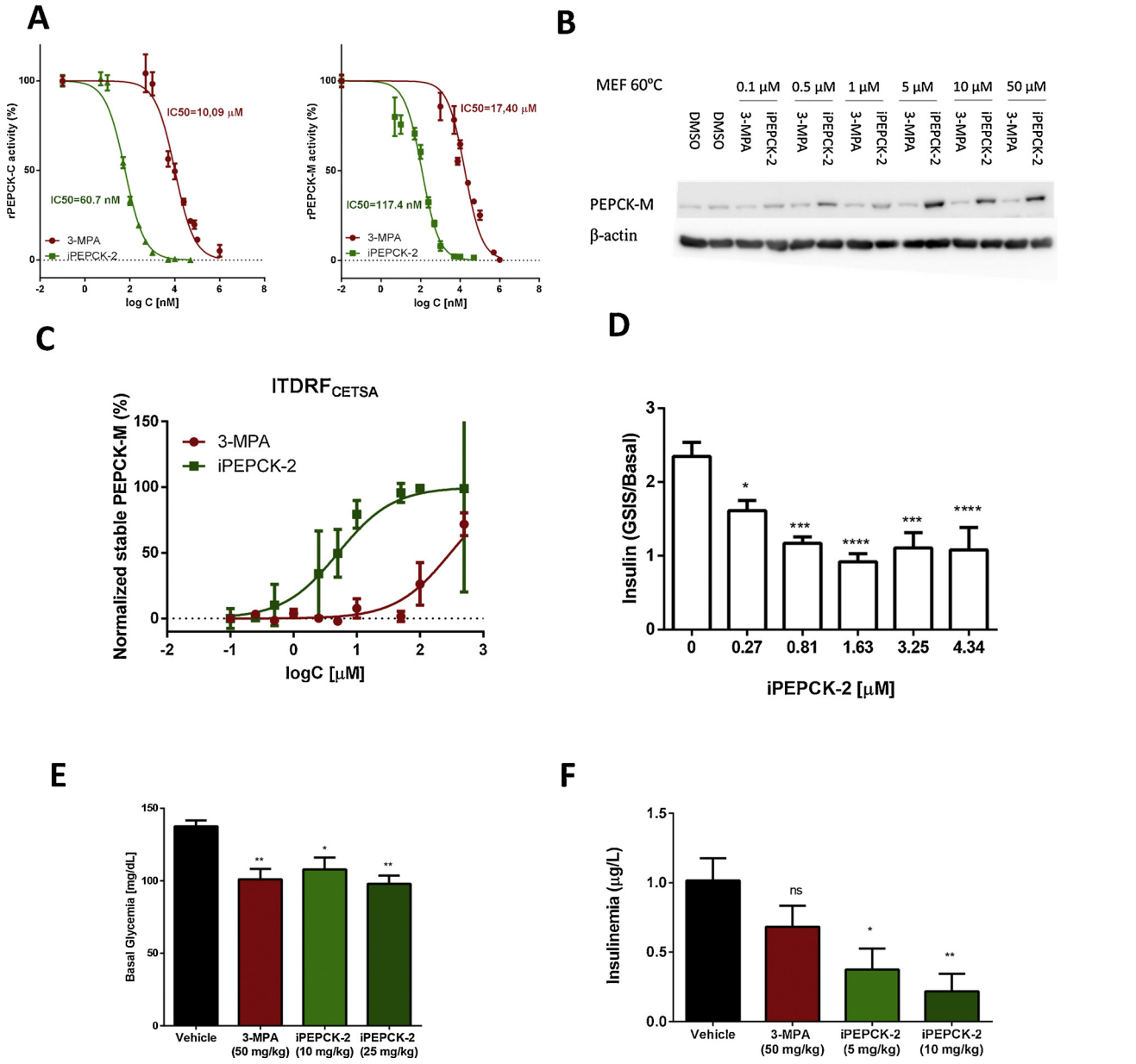

Fig. 2. iPEPCK-2 activity and target engagement. (A) Inhibition of purified human recombinant PEPCK-C and PEPCK-M by iPEPCK-2 and 3-MPA. IC_{50} for both isoforms are noted for every plot. (B) Representative Cellular Thermal Shift Assay (CETSA) at varying concentrations of inhibitors. PEPCK-M specific signal is detected by western blot in MEF cell extracts after 30 min incubation with different concentrations of 3-MPA and iPEPCK-2, prior to thermal treatment at 60 °C. (C) Calculated isothermal dose response fingerprint ($ITDRF_{CETSA}$) for both inhibitors. (D) Effects of iPEPCK-2 and 3-MPA on INS1 glucose-stimulated insulin production shown as a ratio of insulin concentration measured in the presence of 20 mM over 3 mM glucose. (E) Basal glycemia 5 h after an intraperitoneal administration of 3-MPA (50 mg/kg), iPEPCK-2 (10 or 25 mg/kg) or vehicle under fasting conditions. (F) Plasma Insulin at 15 min after an administration of a glucose bolus (2 g/kg) in the presence of inhibitors and vehicle. Data are means ± SEM (3 independent experiments were performed with n ≥ 3 in experiments shown in panels A and D; n ≥ 2 in experiments shown in panels B and C; n = 6 in experiments shown in panels E and F). A one-way Anova and a Sidak multiple comparison test was used. Statistical significance at *p < 0.05, **p < 0.01, ***p < 0.001 *vs* vehicle control.

remaining after 60 min in mice microsomes, predicting good *in vivo* pharmacokinetics (see Table S1 in Supporting Information). This was confirmed in murine *in vivo* pharmacokinetics studies with plasma concentrations of iPEPCK-2 measurable after 15 min of administration and maintained for 8 h, with a C_{max} (0.86 µg/mL or 1405 nM) at 30 min and $t_{1/2\beta}$ at around 2 h (Fig. 1D). The narrow differences in AUC_0^t and AUC_0^∞ showed complete exposure and good bioavailability of iPEPCK-2 after intraperitoneal administration in the described conditions. iPEPCK-2 was not found in the brain at the working concentrations, suggesting that the compound did not cross the blood brain barrier. We classified iPEPCK-2 as to have uncertain BBB permeation based on data from *in vitro* PAMPA assays (Pe value of 2.6 ± 0.2; see Table S2 in Supporting Information). No additional warning on toxicity were measured on cell viability assays in human MRC-5 fibroblast at 100 µM or on hERG inhibition (see Table S3 in Supporting Information). Finally, we found that iPEPCK-2 has acceptable solubility (61 µM at 37 °C in 1% DMSO, 99% PBS).

The inhibitory capacity of iPEPCK-2 and 3-MPA, was assayed on human recombinant PEPCK-C and PEPCK-M produced in our laboratory (Fig. 2A). iPEPCK-2 was the most potent inhibitor for both isoforms with an IC_{50} of 117.4 nM for PEPCK-M and 60.7 nM for the cytosolic isoform. The capacity to reach the mitochondria and inhibit PEPCK-M was confirmed using a cellular thermal shift assay (CETSA) (Fig. 2B). All inhibitors tested thermally stabilized PEPCK-M in live MEF cells,

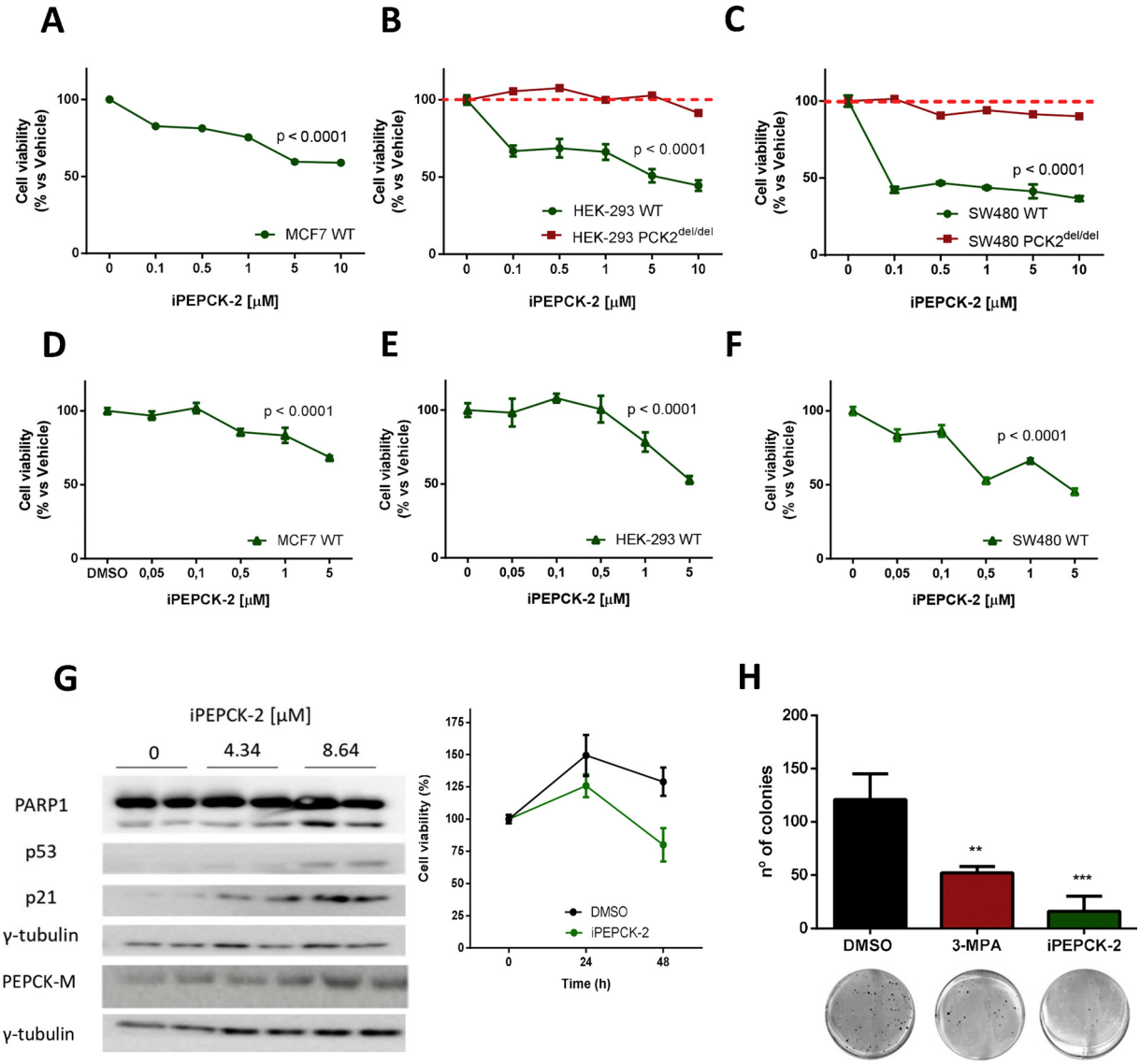

Fig. 3. Target selectivity and validation in cultured cancer cells. (A–C) Proliferation of MCF7 (A), HEK-293 wild-type and PCK2$^{del/del}$ (B) and SW-480 wild-type and PCK2$^{del/del}$ (C) after a 72-h treatment with iPEPCK-2. (D-F) Cell survival of wild-type MCF7 (D), HEK-293 (E) and SW-480 (F) in glucose-free media after 48 -hs of treatment with iPEPCK-2. (G) Survival (right panel) and mechanism of apoptotic cell-death (left panel) because of iPEPCK-2 treatment in limiting glucose conditions in HCT-116 wild-type cells. (H) Colonies formed when MCF7 cells were seeded in soft agar and treated with PEPCK-M inhibitors (5 μM) for 2 weeks. Representative photographs of 2-week colonies formed in each treatment group are noted. Data are means ± SEM (3 independent experiments were performed with n = 5 in each experiment shown in panels A thorough F, and plot shown in panel G; 2 independent experiments were performed with n ≥ 2 to produce the representative western blot shown in panel G; 3 independent experiments were performed with n ≥ 3 to produce panel H plot and representative photographs). A one-way Anova and a Sidak multiple comparison test was used. Statistical significance at *p < 0.05, **p < 0.01, ***p < 0.001 *vs* vehicle control.

which express exclusively the PEPCK-M isoform [7], confirming the accessibility to, and the binding and interaction with PEPCK-M in the mitochondrial matrix by both inhibitors. The capacity of the inhibitors to stabilize PEPCK-M against thermal denaturation was dose-dependent. A quantitative evaluation of target engagement at various doses of inhibitor demonstrated that iPEPCK-2 had the highest affinity for PEPCK-M, as compared to 3-MPA ($ITDRF_{cetsa}$, dose of inhibitor achieving a 50% stabilization at 60°C, was 5.08 *vs* 303.9 μM for iPEPCK-2 and 3-MPA, respectively) (Fig. 2C).

To evaluate the capacity of iPEPCK-2 to inhibit PEPCK-M driven pathways in an *in-cell* assay where PEPCK-C is not present, we took advantage of the role of this isoenzyme relaying glucose metabolism and insulin secretion (GSIS) in pancreatic β-cells or rat insulinoma INS-1, demonstrated using genetic models and oligonucleotides [5]. We therefore characterized iPEPCK-2 inhibition efficiency (EC_{50}) in INS-1 cells by quantifying glucose-stimulated insulin production (GSIS) in the presence of various concentrations of inhibitor. These studies confirmed that iPEPCK-2 treatment inhibited GSIS in a dose-dependent manner with an approximate EC_{50} of 250 nM (Fig. 2D).

To further evaluate the capacity of iPEPCK-2 to antagonize PEPCK driven pathways, we assayed hepatic gluconeogenesis and insulin secretion *in vivo*. Hepatic gluconeogenesis in rodents is mainly driven by PEPCK-C [4,6]. In fasted mice, systemic *in vivo* glucose production is assayed in response to a bolus administration of pyruvate. In this setting, glycemia reflects the net contribution of glucose synthesis to glucose homeostasis. iPEPCK-2 (10 and 25 mg/kg) and 3-MPA (50 mg/kg) had a significant negative impact on basal glycemia 5 -hs after administration (Fig. 2E), and over the glycemia excursion observed after the pyruvate bolus (see Fig. S3A–B in Supporting Information), as compared to DMSO treated mice. These data suggest that 3-MPA and iPEPCK-2 inhibit hepatic gluconeogenesis *in vivo*.

Finally, to assess PEPCK-M specific inhibition *in vivo*, we evaluated

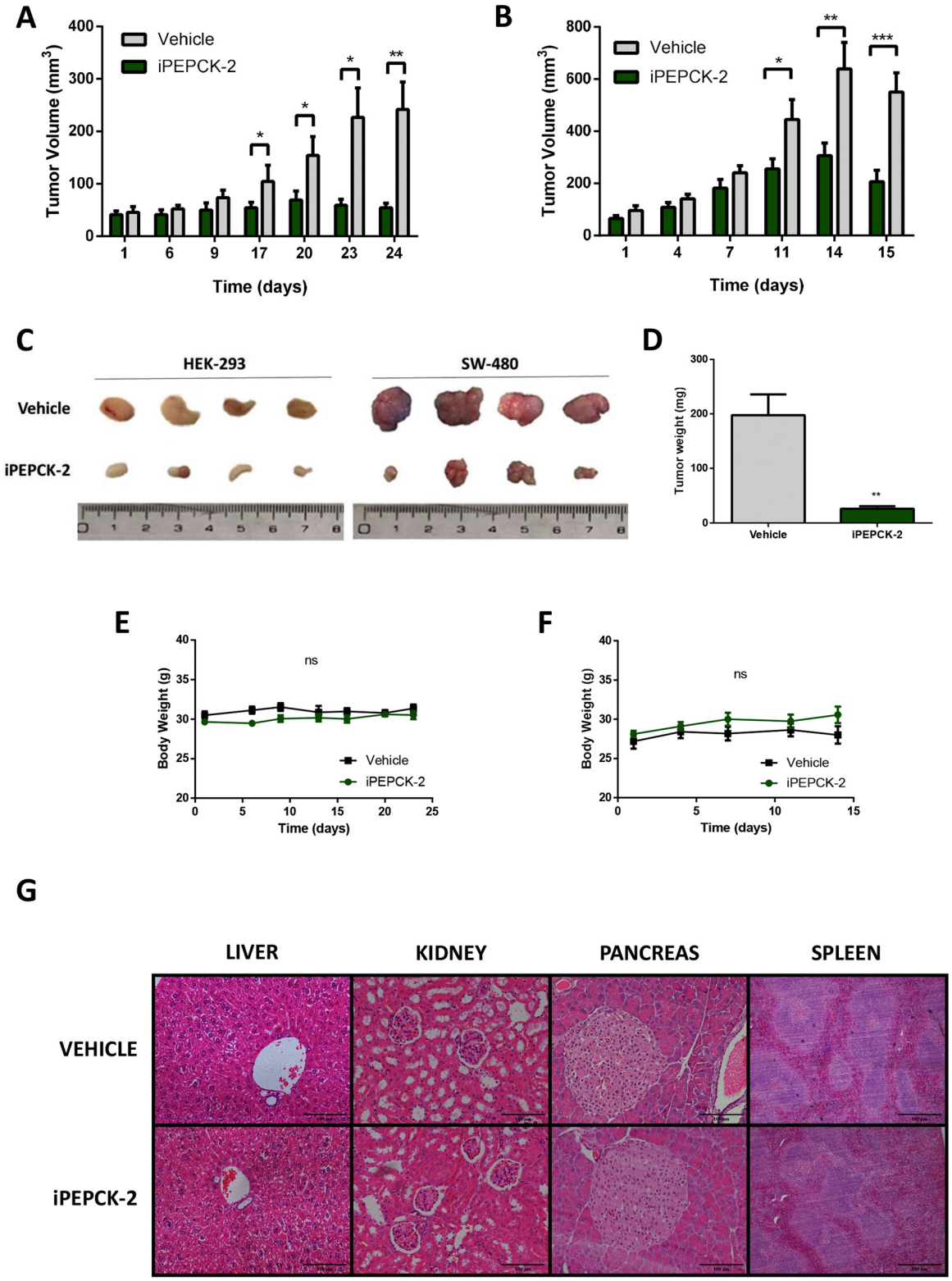

Fig. 4. ***In vivo*** **evaluation of iPEPCK-2 antitumoral activity in two murine subcutaneous xenograft models.** (A–B) Over-the-skin tumor volume ([short length^2 x long length]/2) from HEK-293 (A) and SW-480 (B) cells implanted into the flanks of BALB/C nude mice. Once the tumors grew sufficiently large to be measurable, animals were randomly grouped and daily treated with 8 mg/kg of iPEPCK-2 or vehicle intraperitoneally. (C) Representative tumor explants are shown. (D) HEK-293 tumors were weighted at the time of sacrifice. (E–F) Animals growing HEK-293 (E) and SW-480 (F) tumors were weighted periodically over the course of the experiment to detect health-related issues. (G) Representative H&E stained sections from various organs (liver, kidney, pancreas and spleen) to show no sign of apparent toxicity. Data are means ± SEM (n = 5 in each experiment shown in panels A thorough F, except for HEK-293 control group containing n = 3 due to animal issues upon tumor over growth; at least n = 3 sections per tumor were produced and examined to produced panel G and representative photographs).

pancreatic β-cell secretion of insulin in response to an intraperitoneal glucose bolus (IGTT). In this assay, glucose-stimulated insulin secretion generates a peak of plasma insulin concentration after a 2 g/kg glucose bolus is administered intraperitoneally in fasted mice. The animals for this test were submitted to inhibitor treatment just 2 -hs before the glucose bolus to avoid significant effects on basal glycemia (Fig. S3C). Treatment with iPEPCK-2 (10 mg/kg) showed a blunted insulin secretion response to glucose as compared to vehicle and 3-MPA (50 mg/kg) treated mice (Fig. 2F). The dose of iPEPCK-2 utilized confirmed that a single intraperitoneal administration of 8–10 mg/kg was enough to achieve efficacy, as supported by pharmacokinetic data (Fig. 1D) showing plasma concentrations of the drug 8 h post-administration always above the approximate EC_{50} calculated for insulinoma cells. 3-MPA reduction of insulin secretion was not statistically significant, suggesting inefficient target engagement as compared to the successful targeting of liver PEPCK-C demonstrated in the previous experiment (Figs. 2E and S3A-B; gluconeogenesis), or a problem to successfully reach pancreatic β-cells. Therefore, iPEPCK-2 targets PEPCK-M *in vivo* in pancreas β-cells, but it is non-selective for the mitochondrial isoform (Fig. 2D–F).

3.2. Preclinical validation of iPEPCK-2 and its target in cancer indications

PEPCK-M is present in pancreatic β-cells, tumor cells [5,7] and progenitors (neuroprogenitor cells [8];), hinting at a possible role for the enzyme in cancer cell metabolic adaptations. Indeed, we and others have validated this enzyme as a cancer target in several genetic models, both *in vitro* and *in vivo* [7,10–12]. Therefore, we aimed to validate iPEPCK-2 in a preclinical cancer indication by assaying viability, invasion, and *in vivo* tumor growth using epithelial MCF7 and HEK-293, and human colon carcinoma cells from epithelial HCT-116 and mesenchymal SW-480 origins. These cell lines express high levels of PEPCK-M and the cytosolic isoform is undetectable (Expression Atlas RNAseq geneset E-MTAB-2770). To evaluate target selectivity and test for off-target events, the impact of iPEPCK-2 in tumor cell viability was also assessed in cells lacking PEPCK-M using knock-out clones of HEK-293 (HEK-293-PCK2$^{del/del}$) and SW-480 (SW-480-PCK2$^{del/del}$) previously generated in our laboratory using CRISPR*Cas9* (Fig. S4, and Hyrossova et al, publication pending).

Treatment with iPEPCK-2 significantly reduced DMSO-normalized viability in wild type MCF7, HEK-293, and SW-480 cells grown in optimal culture conditions (Fig. 3A–C). Changes in viability with iPEPCK-2 were dependent on the presence of PEPCK-M, since when tested in HEK-293-PCK2$^{del/del}$ and SW-480-PCK2$^{del/del}$ cells the compound did not show additional effects beyond those consequence of knocking-out the gene, at least within the range of iPEPCK-2 (0.1–10 μM) utilized in the validation assays. All in all, these data suggest target selectivity and a no significant off-target effects (Fig. 3A–C).

PEPCK-M participates in pro-survival mechanisms engaged by nutrient limitation through the ER-stress pathway, and silencing the gene exacerbates ER-stress-mediated apoptosis [7]. Consistently, PEPCK-M inhibitors decreased the DMSO-normalized viability of cancer cells coping with nutrient stress after 48 h of glucose deprivation (Fig. 3D–F). These effects mimicked the consequences of PEPCK-M loss in HEK-293-PCK2$^{del/del}$ and SW-480-PCK2$^{del/del}$ when compared to their wild-type counterparts (Hyrossova et al, publication pending). The inhibition of PEPCK-M with iPEPCK-2 also copied the response observed in genetic models by Mendez-Lucas et al, as iPEPCK-2 compromised growth and enhanced PARP cleavage and apoptosis upon activation of p53 and p21 in HCT-116 cells in limiting glucose conditions (Fig. 3G). A physiologically relevant model to evaluate the response of cancer cells to diffusion constraints in nutrient supply is colony formation and growth in an anchorage-independent manner. Anchorage-independent growth during invasion and metastatic processes is also an important hallmark in cancer progression. iPEPCK-2 and 3-MPA treatment significantly reduced MCF7 colony formation when seeded in soft agar (Fig. 3H), although 3-MPA was less effective. Similar results were obtained in HCT-116 (data not shown).

We next examined the capacity of inhibitor iPEPCK-2 to blunt tumor growth in two xenograft murine models. Colon carcinoma (SW-480) or transformed kidney embryonal cells (HEK-293) cells were subcutaneously injected in both flanks of athymic mice and allowed to grow until measurable at the surface of the skin. Mice were randomly split into two different groups treated with a daily intraperitoneal injection of 8 mg/kg of iPEPCK-2 or vehicle for a variable period depending on the biological features of each model. Whereas vehicle treatment did not impede tumor growth, iPEPCK-2 treatment halted tumor growth in either xenograft mode, as measured both by continuous evaluation of volume under-the-skin and final weight (Fig. 4A–D). Histopathology of tumor samples from treated or untreated breast carcinoma or colon carcinoma tumors showed marked differences in both groups, with prominent necrosis observed in iPEPCK-2 treated tumors and reduced tumor cell burden overall (quantified in Fig. S5A–E in Supporting Information). Furthermore, no signs of apparent toxicity were observed upon close inspection; specifically, there was no macroscopic affectation of the liver or the spleen, weight loss (Fig. 4E and F), lethargy or major health-related disturbance apparent on mucosae or skin quality. The histopathological analysis of eosin and hematoxylin stained tissue sections from different organs did not show any sign of toxicity (Fig. 4G).

4. Discussion

The dominant role of hepatic PEPCK-C in the imbalance of glucose homeostasis in obese and diabetic patients [3] has justified the development of several low-potency compounds targeting this enzyme in the past 30–40 years (Jomain Baum et al., 1976), including compounds that mimic OAA [20], or analogs of 3-MPA [21]. In 2007, Pietranico et al. [13] described a series of C-8 modifications of xanthine derivatives with increased potency against PEPCK-C in the context of diabetes indications, although, it is unclear whether these compounds are being further pursued.

Because of recent findings on the mitochondrial isoform, PEPCK-M, and its impact in cancer biology [22], development of compounds targeting this pathway for cancer indications has gained new interest. Based on the sequence identity (69%) and similarity (82%), we hypothesized that PEPCK-C inhibitory compounds described by Pietranico et al. (synthesized here as iPEPCK-2) would properly dock onto PEPCK-M, especially since the binding pocket is mostly preserved. Consistently, the two orientations predicted from docking calculations for the benzyl-4-sulfonamide-5-chloro-1,3-dimethyl-1*H*-pyrazole moiety matched the arrangement found in the crystallographic ligand in 2GMV (on PEPCK-C), which is characterized by the stacking of the pyrazole ring with the benzene moiety of F530, with a minor deviation on the second case due to the interaction of the sulfonamide group with the guanidine moiety of R570. Notably, this interaction is enabled by the replacement of G570 in PEPCK-C by R in PEPCK-M, it being one of the few differences found close to the binding pocket. These data unveil the possibility to explore selectivity toward PEPCK-M in the future by exploiting the differences in residues located at the edge of the binding site in the two isoforms.

Activity assays on recombinant PEPCK-M and PEPCK-C from human confirmed cross-inhibition by inhibitor iPEPCK-2. IC_{50} values obtained in PEPCK-C activity assays were in the expected range [13], and 2-orders of magnitude lower than 3-MPA [19,23]. Similar potencies were found for PEPCK-C and PEPCK-M, as can be realized from the resemblance of the binding pockets in the two isoforms and the results from docking calculations. Furthermore, thermal stabilization of PEPCK-M by iPEPCK-2 presented similar kinetics to PEPCK-C in *in-cell* conditions, ruling out that compartmentalization of the mitochondrial isoform presents a relevant hinder to target engagement. Mitochondrial targeting was functionally demonstrated in rat insulinoma cells (INS-1) by

asserting the capacity of inhibitor iPEPCK-2 to interfere with glucose-stimulated insulin secretion in a dose-dependent manner. In the same model, Stark et al. [5] had shown an identical response using siRNA-driven down-regulation of PCK2 mRNA, identifying a role for this protein in the coupling mechanism responsible for insulin secretion secondary to the metabolism of glucose. Similarly, effective targeting of PEPCK-M *in vivo* by iPEPCK-2 was corroborated by a higher than 50% impact on short-term insulin secretion in fasted mice after an intraperitoneal administration of glucose, demonstrating the bioavailability of iPEPCK-2. These data provided the first evidence of PEPCK-M druggability in this physiological context, and an initial assessment of iPEPCK-2 usefulness in a pre-clinical setting, as prior data using oligonucleotide silencing of PEPCK-M in rats had not provided evidence for direct action on the healthy pancreas [24]. Overall, PEPCK-M molecular and functional target engagement was appropriately demonstrated both *in vitro*, *in-cell and in vivo*.

Once druggability was confirmed, iPEPCK-2 was further validated as an anticancer strategy starting off by contrasting the consequences of pharmacological inhibition and genetic ablation using PCK2-KO models produced using CRISPR/*Cas9*. Importantly, PCK2-KO cells also allowed us to demonstrate that the effects on tumor cell growth are PEPCK-M dependent, since iPEPCK-2 was ineffective at altering growth rates at concentrations utilized throughout the study in the absence of PEPCK-M, discarding off-target effects with consequences on tumor biology. In HEK-293 and SW-480 PEPCK-M inhibition by iPEPCK-2 mimicked genetic down-regulation of PEPCK-M by reducing cell proliferation and increasing cell death (not shown; Méndez-Lucas et al., 2014). Finally, even though PEPCK-C has been also implicated in metabolic adaptations specifically in melanoma [25], the participation of this isozyme in some of the effects observed here can be ruled-out as all cancer cell lines utilized in the present study have null expression of this isoform (Expression Atlas RNAseq geneset E-MTAB-2770). All-in-all, these data suggest that PEPCK-M is the plausible target for iPEPCK-2 in tumor cells at the concentrations tested.

Its potential as anticancer target resides in the capacity of PEPCK-M to flux glutamine carbons entering the TCA towards the glycolytic pool for the synthesis or serine/glycine, especially under nutrient deprivation, balancing ER stress and increasing cell survival [6,7,10]. This is exemplified in the marked effects observed after PEPCK-M inhibition in anchorage-independent growth in soft-agar, further validating PEPCK-M role in tumor cell metabolism, but also in invasiveness and metastasis. This idea was reinforced *in vivo* where both xenografted tumors stalled by daily administration of iPEPCK-2 as compared with vehicle. Reduced tumor growth confirmed that PEPCK-M expression offers a growth advantage to cancer cells and its inhibition could be a useful anticancer strategy. Pharmacokinetics profile and good bioavailability, with no crossing of the BBB, are good starting grounds for the prospective use of this compound in further clinical testing. Importantly, possible toxicity issues secondary to the inhibition of liver PEPCK-C or pancreatic PEPCK-M were not substantiated in xenografted mice by our limited evaluation of liver histology, weight gain or other health related signs, or changes in plasma insulin or glucose (Fig. S5F–G). Besides, insulin being a well-known growth factor, reduced insulinemia could work in synergy with PEPCK-M inhibition in the tumor. However, a full-blown toxicity assessment will be required to confirm these claims in the future.

In summary, we report here the first validation of a compound that target PEPCK-M as cancer therapeutics. PEPCK-M's crucial role in conditions of glucose limitation are accompanied by the capacity of the pathway to balance ER-stress and amino acid availability to warrant the anticancer effectiveness of iPEPCK-2 in our xenografted models. Hence, PEPCK-M is an exceptional element of the tumor metabolic toolbox to cope with huge variations in nutrient and metabolite availability in the heterogenous tumor. As clinical evidence mounts on the relevance of targeting metabolic enzymes for cancer therapy, it is indeed becoming clearer that pursuing key tumor metabolic hallmarks such as glycolysis or glutamine addiction might not be enough in the long run [26]. Therefore, a double-sword strategy, where PEPCK-M is one of the hits, might be ideal to deal with the demonstrated metabolic flexibility of tumors cells.

Ethics statement for research with animals

All animals were treated according to protocols approved by the Department of the Environment and Housing (DMAH, Generalitat de Catalunya, Spain) in an SPF housing facility located at the IDIBELL/Bellvitge Campus of the University of Barcelona with free access to food and water under a physiological light/dark cycle. No breeding was necessary for the experimental procedures described and all animals were provided by commercial vendors prior to utilization. A one-week adaptation period was allowed before handling for experimental procedures. The research was conducted in compliance with the Spanish legislation on "Protection of Animals Used for Experimental and Other Scientific Purposes" and in accordance with the EU Directive 2010/63/EU on this subject. Besides, the study complies with the ARRIVE guidelines developed by the NC 3Rs and the efforts to reduce the number of subjects used.

Consent for publication

N/A.

Data availability

No datasets were generated in the course of the work presented here, therefore data archival does not apply for this study. All data is available from the authors, and will be archived for a certain amount of time subject to regulations by the Institution (University of Barcelona).

Funding

This work was supported by grants from the Spanish "Ministerio de Economia y Competitividad" (MINECO; BFU2015-66030-R and SAF2017-85869-R) to JCP and FV, respectively (co-funded by the European Regional Development Fund, ERDF, A Way to Build Europe), and with support by Secretariat for Universities and Research of the Department of Business and Knowledge of the Government of Catalonia (2017SGR106, 2017SGR204, 2017SGR449 and 2017SGR1746). We are indebted to the "Ministerio de Educación" FPU and the "Ministerio de Economia y Competitividad" (MINECO) FPI for financial support for PH and JMF, respectively, and to the Generalitat de Catalunya FI program for partial financial support for MA and SRA, and the CERCA Program/Generalitat de Catalunya for their institutional support to IDIBELL.

Author contributions

MA: performed experiments, collected and analyze data. Wrote the manuscript.

JMF: performed experiments, collected and analyze data, and discussed the preliminary draft and provided feedback on general and specific details of the manuscript.

SA: performed experiments, collected and analyze data.

SRA: performed experiments, collected and analyze data.

PH: performed experiments, collected and analyze data, and discussed the preliminary draft and provided feedback on general and specific details of the manuscript.

AF: performed experiments, collected and analyze data, and discussed the preliminary draft and provided feedback on general and specific details of the manuscript.

FV: analyzed data, discussed the preliminary draft and provided feedback on general and specific details of the manuscript.

BP. performed experiments, collected and analyze data, and

discussed the preliminary draft and provided feedback on general and specific details of the manuscript.

MIL: analyzed data, discussed the preliminary draft and provided feedback on general and specific details of the manuscript.

JB: analyzed data, discussed the preliminary draft and provided feedback on general and specific details of the manuscript.

PL: contributed original materials, discussed the preliminary draft and provided feedback on general and specific details of the manuscript

JAC: contributed original materials, discussed the preliminary draft and provided feedback on general and specific details of the manuscript

PMGR: discussed the preliminary draft and provided feedback on general and specific details of the manuscript

CG: discussed the preliminary draft and provided feedback on general and specific details of the manuscript

TG: performed experiments, collected and analyze data.

FJL: analyzed data, discussed the preliminary draft and provided feedback on general and specific details of the manuscript. Conceived of the work.

CE: analyzed data, discussed the preliminary draft and provided feedback on general and specific details of the manuscript. Conceived of the work.

JCP: analyzed data, discussed the preliminary draft and provided feedback on general and specific details of the manuscript. Conceived of the work. Wrote the manuscript.

Declaration of Competing Interest

We declare no conflict of interest, financial or otherwise, in relation to the work described here.

Acknowledgements

We acknowledge the skillful technical support by the Scientific and Technical Services at the University of Barcelona, Bellvitge Campus, and to the “Consorci de Serveis Universitaris de Catalunya” (CSUC) for computational facilities.

Appendix A. Supplementary data

Supplementary material related to this article can be found, in the online version, at doi:https://doi.org/10.1016/j.biopha.2019.109601.

References

[1] H.C. Chang, M.D. Lane, The enzymatic carboxylation of phosphoenolpyruvate. II. Purification and properties of liver mitochondrial phosphoenolpyruvate carboxykinase, J. Biol. Chem. 241 (1966) 2413–2420.

[2] R.C. Nordlie, H.A. Lardy, Mammalian liver phosphoneolpyruvate carboxykinase activities, J. Biol. Chem. 238 (1963) 2259–2263.

[3] R.W. Hanson, A.J. Garber, Phosphoenolpyruvate carboxykinase. I. Its role in gluconeogenesis, Am. J. Clin. Nutr. 25 (1972) 1010–1021.

[4] J. Semakova, P. Hyroššová, A. Méndez-Lucas, E. Cutz, J. Bermudez, S. Burgess, S. Alcántara, J.C. Perales, PEPCK-C reexpression in the liver counters neonatal hypoglycemia in Pck1 $^{del/del}$ mice, unmasking role in non-gluconeogenic tissues, J. Physiol. Biochem. 73 (2017), https://doi.org/10.1007/s13105-016-0528-y.

[5] R. Stark, F. Pasquel, A. Turcu, R.L. Pongratz, M. Roden, G.W. Cline, G.I. Shulman, R.G. Kibbey, Phosphoenolpyruvate cycling via mitochondrial phosphoenolpyruvate carboxykinase links anaplerosis and mitochondrial GTP with insulin secretion, J. Biol. Chem. 284 (2009) 26578–26590, https://doi.org/10.1074/jbc.M109.011775.

[6] A. Méndez-Lucas, J.A.G. Duarte, N.E. Sunny, S. Satapati, T. He, X. Fu, J. Bermúdez, S.C. Burgess, J.C. Perales, PEPCK-M expression in mouse liver potentiates, not replaces, PEPCK-C mediated gluconeogenesis, J. Hepatol. 59 (2013) 105–113, https://doi.org/10.1016/j.jhep.2013.02.020.

[7] A. Méndez-Lucas, P. Hyroššová, L. Novellasdemunt, F. Viñals, J.C. Perales, Mitochondrial phosphoenolpyruvate carboxykinase (PEPCK-M) is a pro-survival, endoplasmic reticulum (ER) stress response gene involved in tumor cell adaptation to nutrient availability, J. Biol. Chem. 289 (2014) 22090–22102, https://doi.org/10.1074/jbc.M114.566927.

[8] Z. Alvarez, P. Hyrossova, J.C. Perales, S. Alcantara, Neuronal progenitor maintenance requires lactate metabolism and PEPCK-M-directed cataplerosis, Cereb. Cortex. 26 (2016), https://doi.org/10.1093/cercor/bhu281.

[9] K. Leithner, A. Triebl, M. Trötzmüller, B. Hinteregger, P. Leko, B.I. Wieser, G. Grasmann, A.L. Bertsch, T. Züllig, E. Stacher, A. Valli, R. Prassl, A. Olschewski, A.L. Harris, H.C. Köfeler, H. Olschewski, A. Hrzenjak, The glycerol backbone of phospholipids derives from noncarbohydrate precursors in starved lung cancer cells, Proc. Natl. Acad. Sci. 115 (2018) 6225–6230, https://doi.org/10.1073/pnas.1719871115.

[10] E.E. Vincent, A. Sergushichev, T. Griss, M.-C. Gingras, B. Samborska, T. Ntimbane, P.P. Coelho, J. Blagih, T.C. Raissi, L. Choinière, G. Bridon, E. Loginicheva, B.R. Flynn, E.C. Thomas, J.M. Tavaré, D. Avizonis, A. Pause, D.J.E. Elder, M.N. Artyomov, R.G. Jones, Mitochondrial phosphoenolpyruvate carboxykinase regulates metabolic adaptation and enables glucose-independent tumor growth, Mol. Cell 60 (2015) 195–207, https://doi.org/10.1016/j.molcel.2015.08.013.

[11] J.-W. Park, S.C. Kim, W.K. Kim, J.P. Hong, K.-H. Kim, H.Y. Yeo, J.Y. Lee, M.S. Kim, J.H. Kim, S.Y. Yang, D.Y. Kim, J.H. Oh, J.Y. Cho, B.C. Yoo, Expression of phosphoenolpyruvate carboxykinase linked to chemoradiation susceptibility of human colon cancer cells, BMC Cancer 14 (2014) 1–24, https://doi.org/10.1186/1471-2407-14-160.

[12] K. Leithner, A. Hrzenjak, M. Trötzmüller, T. Moustafa, H.C. Köfeler, C. Wohlkoenig, E. Stacher, J. Lindenmann, L. Harris, A. Olschewski, H. Olschewski, PCK2 activation mediates an adaptive response to glucose depletion in lung cancer, Oncogene 34 (2015) 1044–1050, https://doi.org/10.1038/onc.2014.47.

[13] S.L. Pietranico, L.H. Foley, N. Huby, W. Yun, P. Dunten, J. Vermeulen, P. Wang, K. Toth, G. Ramsey, M.-L. Gubler, S.J. Wertheimer, C-8 modifications of 3-alkyl-1,8-dibenzylxanthines as inhibitors of human cytosolic phosphoenolpyruvate carboxykinase, Bioorg. Med. Chem. Lett. 17 (2007) 3835–3839, https://doi.org/10.1016/j.bmcl.2007.05.013.

[14] A. Waterhouse, M. Bertoni, S. Bienert, G. Studer, G. Tauriello, R. Gumienny, F.T. Heer, T.A.P. de Beer, C. Rempfer, L. Bordoli, R. Lepore, T. Schwede, SWISS-MODEL: homology modelling of protein structures and complexes, Nucleic Acids Res. 46 (2018) W296–W303, https://doi.org/10.1093/nar/gky427.

[15] G.M. Morris, R. Huey, W. Lindstrom, M.F. Sanner, R.K. Belew, D.S. Goodsell, A.J. Olson, AutoDock4 and AutoDockTools4: automated docking with selective receptor flexibility, J. Comput. Chem. 30 (2009) 2785–2791, https://doi.org/10.1002/jcc.21256.

[16] M. Escós, P. Latorre, J. Hidalgo, R. Hurtado-Guerrero, J.A. Carrodeguas, P. López-Buesa, Kinetic and functional properties of human mitochondrial phosphoenolpyruvate carboxykinase, Biochem. Biophys. Rep. 7 (2016) 124–129, https://doi.org/10.1016/j.bbrep.2016.06.007.

[17] R. Jafari, H. Almqvist, H. Axelsson, M. Ignatushchenko, T. Lundbäck, P. Nordlund, D.M. Molina, The cellular thermal shift assay for evaluating drug target interactions in cells, Nat. Protoc. 9 (2014) 2100–2122, https://doi.org/10.1038/nprot.2014.138.

[19] M. Jomain Baum, V.L. Schramm, R.W. Hanson, Mechanism of 3 mercaptopicolinic acid inhibition of hepatic phosphoenolpyruvate carboxykinase (GTP), J. Biol. Chem. 251 (1976) 37–44.

[20] R.M. Stiffin, S.M. Sullivan, G.M. Carlson, T. Holyoak, Differential inhibition of cytosolic PEPCK by substrate analogues. Kinetic and structural characterization of inhibitor recognition, Biochemistry 47 (2008) 2099–2109, https://doi.org/10.1021/bi7020662.

[21] M.D. Balan, M.J. Mcleod, W.R. Lotosky, M. Ghaly, T. Holyoak, Inhibition and allosteric regulation of monomeric phosphoenolpyruvate carboxykinase by 3-mercaptopicolinic acid, Biochemistry 54 (2015) 5878–5887, https://doi.org/10.1021/acs.biochem.5b00822.

[22] G. Grasmann, E. Smolle, H. Olschewski, K. Leithner, Gluconeogenesis in cancer cells – repurposing of a starvation-induced metabolic pathway? Biochim. Biophys. Acta – Rev. Cancer 1872 (2019) 24–36, https://doi.org/10.1016/j.bbcan.2019.05.006.

[23] J.A. Urbina, C.E. Osorno, A. Rojas, Inhibition of phosphoenolpyruvate carboxykinase from Trypanosoma (Schizotrypanum) cruzi epimastigotes by 3-mercaptopicolinic acid: in vitro and in vivo studies, Arch. Biochem. Biophys. 282 (1990) 91–99.

[24] R. Stark, F. Guebre-Egziabher, X. Zhao, C. Feriod, J. Dong, T.C. Alves, S. Ioja, R.L. Pongratz, S. Bhanot, M. Roden, G.W. Cline, G.I. Shulman, R.G. Kibbey, A role for mitochondrial phosphoenolpyruvate carboxykinase (PEPCK-M) in the regulation of hepatic gluconeogenesis, J. Biol. Chem. 289 (2014) 7257–7263, https://doi.org/10.1074/jbc.C113.544759.

[25] Y. Li, S. Luo, R. Ma, J. Liu, P. Xu, H. Zhang, K. Tang, J. Ma, Y. Zhang, X. Liang, Y. Sun, T. Ji, N. Wang, B. Huang, Upregulation of cytosolic phosphoenolpyruvate carboxykinase is a critical metabolic event in melanoma cells that repopulate tumors, Cancer Res. 75 (2015) 1191–1196, https://doi.org/10.1158/0008-5472.CAN-14-2615.

[26] C. Vernieri, S. Casola, M. Foiani, F. Pietrantonio, F. de Braud, V. Longo, Targeting cancer metabolism: dietary and pharmacologic interventions, Cancer Discov. 6 (2016) 1315–1333, https://doi.org/10.1158/2159-8290.CD-16-0615.